Polygonization and anomalous graphene interlayer spacing of multi-walled carbon nanofibers

Mina Yoon,[1,2] Jane Howe,[1] Gary Tibbetts,[3] Gyula Eres,[1] and Zhenyu Zhang[1,2]
[1]*Materials Science and Technology Division, Oak Ridge National Laboratory, Oak Ridge, Tennessee 37831, USA*
[2]*Department of Physics and Astronomy, The University of Tennessee, Knoxville, Tennessee 37996, USA*
[3]*Applied Sciences Inc., P.O. Box 579, Cedarville, Ohio 45314, USA*
(Received 5 January 2007; published 2 April 2007)

The graphene interlayer spacing in pure graphite is known to have a minimum value of d_{min}=0.3354 nm, while defective graphites typically have larger interlayer spacings. Using x-ray diffraction, we find that the graphene interlayer spacing in multi-walled carbon nanofibers heat treated above ≈2800 K is distinctly smaller than d_{min}. To explain this unusual observation, we investigate the structural properties of carbon nanotubes using a multiscale approach rooted in extensive first-principles calculations, specifically allowing the nanotube cross sections to polygonize. We show that, whereas normal nanotubes are favored energetically at low temperatures, the configuration entropy associated with Stone-Wales defect creation at high temperatures makes the polygonal shape of large nanotubes or nanofibers thermodynamically stable, accompanied by a reduction in the graphene interlayer spacing. These unique predictions are confirmed in further experimental tests.

DOI: 10.1103/PhysRevB.75.165402 PACS number(s): 81.07.De, 61.46.−w, 64.70.Nd, 68.37.Lp

I. INTRODUCTION

Recent discoveries of low-dimensional carbon materials, such as fullerenes[1] and nanotubes,[2] have generated much research effort in exploring their physical and chemical properties. In particular, a fundamental understanding of their structural properties is essential in order to fully utilize their device potentials in nanotechnology.

For several different types of carbon-based nanostructures, one fundamental quantity is the graphene interlayer spacing, corresponding to the d_{002} peak observed in x-ray diffraction (XRD). This quantity has a broadly accepted minimum value of d_{min}=0.3354 nm (Ref. 3) for single-crystal graphites having true *ABAB* stacking.[4] This prevailing view has led to the classification of a variety of "graphitic" materials, ranging from those with good *ABAB* stacking and d_{002} near 0.335 nm (Ref. 3) to "turbostratic" materials with no interplanar ordering and d_{002} up to 0.344 nm.[5] For example, when graphene layers roll up to form multi-walled carbon nanotubes (MWCNTs), the interlayer spacing increases exponentially from d_{min} as the tube radius decreases.[6]

There are a few notable exceptions of graphites reported to have d_{002} values lower than d_{min}.[7–9] The earliest examples were "Kish" graphites deposited on the surfaces of molten steel, which show a d_{002} value of 0.33528 nm.[7] However, molten steel was known to contain abundant Fe and Si impurities, which evidently applied a high internal pressure to the Kish graphite. After removing the impurities by either heat treatment or acid washing, the lattice spacing expanded back to the nominal value of graphite.[7] More recently, it was reported that heat treatment of a mixture of demineralized anthracite and minerals such as rutile (TiO_2), calcite ($CaCO_3$), or hematite (Fe_2O_3) leads to graphene interlayer spacings of 0.3352, 0.3350, or 0.3349 nm, respectively (±0.0001 nm).[8] Furthermore, applying high external pressure or high-energy electron irradiation could cause a significant reduction in the interlayer spacing of graphite or a confined structure such as a spherical shell and, ultimately, could induce a transition to diamond.[9]

In this paper, we establish a different experimental approach for inducing reductions in the graphene interlayer spacing—high-temperature treatment—and rationalize the observation within a unified theoretical model of carbon nanotubes. First, using x-ray diffraction, we find that the graphene interlayer spacing in multi-walled carbon nanofibers heat treated above ≈2800 K is distinctly smaller than d_{min}. The model developed is multiscale in nature, and is characterized by the introduction of a local curvature that allows the nanotube cross sections to polygonize. We show that, whereas normal nanotubes are favored energetically at low temperatures, the configuration entropy associated with Stone-Wales (SW) defects can make the polygonal shape of the large nanotubes or nanofibers metastable at intermediate temperatures, and globally favorable at sufficiently high temperatures. Furthermore, such polygonal carbon nanotubes exhibit clear reductions in the graphene interlayer spacing. These predictions are convincingly confirmed in further experimental studies of carbon nanofibers with varying cross sections and at different heat treatment temperatures.

The paper is organized as follows. In Sec. II, we first explain the experimental procedures used in the sample preparation and measurements of the multi-walled carbon nanofibers, followed by a presentation of the experimental observation of the interlayer spacing reduction of the multi-walled carbon nanofibers. In Sec. III, we present the theoretical modeling approach used to explain the experimental observations. In Sec. IV, we explore possible mechanisms of interlayer spacing reduction of multi-walled carbon nanofibers or nanotubes. Our study shows that interlayer spacing reduction can be observed in polygonized nanofibers or nanotubes. In Sec. V, we present additional experiments confirming the theoretical prediction of polygonization in the carbon nanofiber samples. In Sec. VI, we present our conclusion.

 ©2007 The American Physical Society

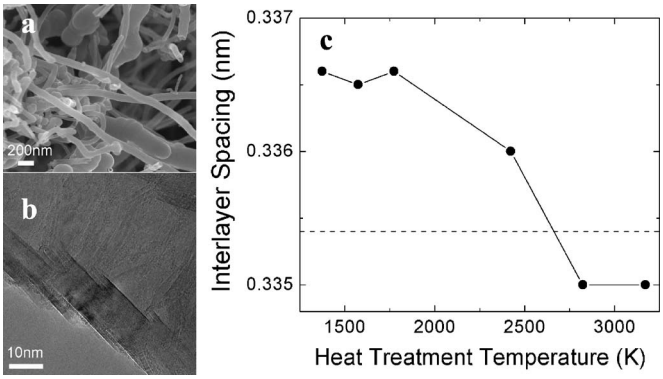

FIG. 1. SEM (a) or TEM (b) image showing that as-grown fibers have circular cross sections (a) and heat-treated fibers are well graphitized (b). (c) Experimentally measured interlayer spacing of the fibers as a function of the heating temperature (Ref. 28). The dotted line marks the spacing of natural graphite. The error bar is within 4×10^{-5} nm, smaller than the size of the data points.

II. EXPERIMENTAL OBSERVATION OF INTERLAYER SPACING REDUCTION OF MULTI-WALLED CARBON NANOFIBERS

The carbon nanofibers studied here were approximately 100 nm in diameter, with an average initial aspect ratio exceeding 100. The fibers were produced by Applied Sciences, Inc. (PYROGRAF PR-24 and PR-19, see http://www.apsci.com) in a flow of natural gas, air, ammonia, and the catalytic constituents hydrogen sulfide and iron pentacarbonyl. The as-grown fibers had a duplex morphology comprised of an inner core, which was deposited by an Fe-based catalytic particle, covered with a layer of vapor-deposited turbostratic carbon. These fibers were heat treated under Ar in a furnace that used a graphite heating element. Different batches of fibers were treated at 3000, 3100, and 3500 K, respectively. The MWCNTs were heat treated at 3037 K for 1 h in a similar furnace. The microstructures of the fibers before and after heat treatment up to ≈3500 K were examined using transmission electron microscopy (TEM) and scanning electron microscopy (SEM). The as-grown fibers had the geometry of stacked cups, with circular cross sections, as seen in the SEM image [Fig. 1(a)]. After heat treatment, such fibers were well graphitized, as shown in the TEM image [Fig. 1(b)].

To measure the interlayer spacing of the nanofibers, XRD was carried out using a Sintag PAD diffractometer with Cu $K\alpha$ x-radiation. The results are shown in Fig. 1(c). The as-grown nanofibers were placed in a furnace and warmed to each target temperature where they were held for 1 h. Then the fibers were cooled down to room temperature for measurement.[10] The samples heat treated with $T\leqslant2500$ K showed a moderate interlayer spacing expansion, $d_{002}\geqslant0.336$ nm. As the temperature reached ≈2800 K, the measured interlayer spacing became 0.3350 nm, reduced from that of natural graphite [0.3354 nm, corresponding to the dotted line in Fig. 1(c)]. Further increases in heat temperature led to the same degree of reduction to within the experimental error of 4×10^{-5} nm [the error bars are within the size of the data points in Fig. 1(c)]. The stable reduction was observed all the way up to 3500 K, the highest heating temperature reached in our experiments.

TEM and XRD studies confirmed that the stacked-cup nanofiber samples contained no metal impurities. Furthermore, the samples were neither exposed to electron irradiation nor to external pressure; therefore, none of the existing mechanisms can be invoked to explain the interlayer spacing reduction observed here. An obvious difference between ideal planar graphene and nanotube and/or nanofiber structures is the existence of finite curvatures in the latter case. Nevertheless, as shown in Ref. 6 and in the data in Fig. 1(c) with $T\leqslant2800$ K, standard carbon nanotubes or nanofibers only exhibit increased interlayer spacings over d_{min}.

III. THEORETICAL MODELING: METHODS

The above observations motivated us to investigate theoretically the feasibility that the nanofibers develop polygonal cross sections under high-temperature heat treatment, and in turn, the corresponding increase in the local curvature associated with the polygonal deformation causes a reduction in the interlayer spacing. To explore this feasibility, we first developed a unified model of MWCNTs and polygonal nanotubes (PNTs) without considering the effects of temperature. Consider a PNT consisting of piecewise flat graphite sides with N_p edges. A conventional CNT can be viewed as a special case of such a PNT, in which each flat piece has the shortest possible length of $w_0=0.5a$, with $a=0.244$ nm. We introduce[11]

$$K_l(p)=\frac{1}{K_0}\left(\frac{\pi-\theta_p}{\sin\theta_p}-1\right) \tag{1}$$

to describe the local curvature at any vertex point p of the cross section of a nanotube, with θ_p the interplanar angle at point p, and the normalization factor $K_0=(4\pi/3\sqrt{3})-1$ for zigzag edged nanotubes and $K_0=(\pi/\sqrt{3})-(3/4)$ for armchair edged nanotubes.

When wrapping up graphitic layers, the spatial restriction imposed by the wrapping will prevent the formation of perfectly graphitized structures with optimum interlayer spacings, because it is atomically impossible to satisfy perfect atomic registry for all the layers.[12] Here the perfect atomic registry refers to the AB stacking, with a maximal energy gain in the interlayer attraction between two neighboring layers. As a result, all the physical quantities will be obtained by taking an ensemble average over large samples. To search for the mechanism that may likely cause an interlayer spacing reduction, we considered a buckled graphite bilayer, whose adjacent layers can maintain identical local curvatures. The bilayer can be either AB or AA stacked, periodically repeated in the planar directions with a sufficiently large vacuum spacing layer in the z direction [see the top panel in Fig. 2(a)]. Using such structural models, we are able to describe the energetics of a PNT and the optimum interlayer spacing of a multi-walled polygonal nanotube (MWPNT).

Our total energy calculations are based on the local-density approximation (LDA) within density-functional theory (DFT), as implemented in the VASP code.[13] We use an

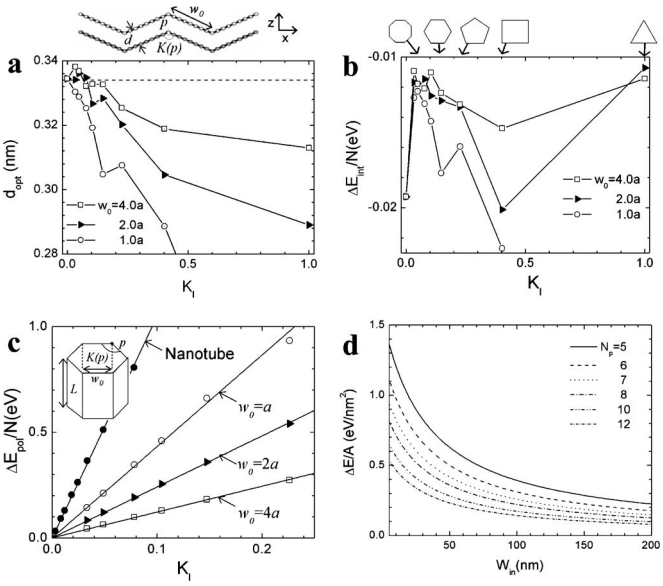

FIG. 2. The buckled-graphite model considered to investigate the role of the local curvature (K_l) in determining interlayer interactions as shown on top of (a). The structures are stacked in *AA* or *AB* fashion and extend in three dimensions. (a) The optimum interlayer spacing (d_{opt}) as a function of the local curvature. (b) The energy difference (ΔE_{int}) between the structure shown on top of (a) and that of the same two layers but with an infinite separation. (c) Formation energy [Eq. (2)] of single-walled polygonal nanotubes as a function of the local curvature. The solid lines are fits using Eq. (2) to the data points from LDA-DFT calculations. The inset illustrates a polygonal nanotube consisting of N_p piecewise flat sides, with N_p=6. (d) Energy cost (ΔE) per unit area to make 30-walled polygonal nanotubes relative to the energy of a circular nanotube as a function of the innermost tube width (W_{in}) and the polygon order (N_p).

ultrasoft pseudopotential[14] and employ the Ceperley-Alder exchange correlation[15] as parametrized by Perdew and Zunger.[16] The energy cutoff for the plane-wave basis set is 550 eV and Monkhorst-Pack *k*-point sampling[17] is used. We note that there has been a successful effort at going beyond the LDA when describing van der Waals interactions.[18] Nevertheless, existing results of LDA-DFT calculations of the in-plane and *c*-axis lattice constants of graphite are in excellent agreement with experimental values.[19] Our own LDA calculations yield an equilibrium in-plane constant a =0.244 nm and an interlayer spacing equal to 0.3343 and 0.3660 nm for graphites with *AB* and *AA* stackings, respectively, again in excellent agreement with other theoretical and experimental results.[19] We therefore limit ourselves to DFT-LDA calculations when studying the optimum interlayer spacing for PNTs with $K_l > 0$.

IV. THEORETICAL MODELING: RESULTS

A. Interlayer spacing reduction of multi-walled nanofibers

For a given bilayer of w_0 and K_l [Fig. 2(a)], the total energy calculation is performed by varying the interlayer spacing d, and the Birch-Murnaghan equation of state[20] is applied to obtain the optimum interlayer distance d_{opt}. The results are presented in Figs. 2(a) and 2(b), corresponding to either *AA* or *AB* stacking,[12] depending on which configuration gives a higher energy gain due to interlayer attraction. The interlayer interaction energy (ΔE_{int}) in Fig. 2(b) measures the energy difference between the structure shown in the top panel in Fig. 2(a) and that of the same two layers but with an infinite separation. Figure 2(a) clearly illustrates that a reduction in the graphene interlayer spacing occurs as the local curvature increases over $K_l > 0.12$. The structures with $w_0=4a$ and $2a$ show small spacing increases for curvatures between $K_l=0.02$ and $K_l=0.12$, but from Fig. 2(b), we see that the interlayer attraction is stronger at larger curvatures. Based on Fig. 2(b), we conclude that polygons with stronger interlayer attractions (such as squares and pentagons) might be preferred.

B. Polygonization of multi-walled nanofibers

To address the feasibility of polygonization of nanotubes with larger cross sections, we have to invoke empirical potentials, as first-principles calculations are limited to only small systems such as those shown in Figs. 2(a) and 2(b). For larger structures, we employ a multiscale scheme, where a PNT is described as a rolled continuous sheet of length L having a total width W ($=w_0N_p$) [see the inset of Fig. 2(c)]. We introduce the following formula to describe the energy difference between a single-walled PNT (SWPNT) and a planar graphene layer:

$$\Delta E_{pol}/L = \sum_{p=1}^{N_p} \varepsilon(p,w_0)K_l(p), \tag{2}$$

where p is the vertex index, $K_l(p)$ is the local curvature, and the coefficient is given by $\varepsilon(p,w_0) = \varepsilon_0[(1-\exp[-[w_0(p)-w_c]/\sigma])^2-1]+\varepsilon_1$, with ε_0 =6.157 eV/nm, ε_1=46.264 eV/nm, w_c=0.2 nm, and σ =0.096 nm. The parameters are obtained by fitting the energy changes obtained from DFT-LDA calculations for small systems, including conventional nanotubes and polygonal structures with $N_p \geqslant 5$ as marked by the data points in Fig. 2(c). Given the excellent fitting of the DFT-LDA results by Eq. (2) for the smaller systems, it is reasonable to use Eq. (2) to estimate the energetics of larger systems as well. Figure 2(d) shows the energy (ΔE) of a N_w-walled PNT per unit area relative to that of a circular MWCNT as a function of the inner tube circumference W_{in}, where the optimum interlayer spacing is 0.34 nm, and N_w is chosen to be 30, close to the number in the experimental observations. The energy required for the formation of polygons decreases with the tube circumference; for a given tube circumference, the formation energy is lower for higher orders of polygons. Most importantly, conventional nanotubes are always the most stable structures if only the different structural energies are compared.

Next, we consider the possible role of defect creation on the MWCNTs,[21] in particular, at finite temperatures. It is known that exposure to high-energy electron irradiation could cause a significant number of vacancies or even fatally

damage the material, but such a process did not take place in our experiments; instead, we mainly focused on the thermally induced creation of defects on the MWCNTs at high temperatures, T. The defect creation rate can be described by $\nu \exp(-V_a/k_B T)$, where V_a is the activation barrier for creating a given type of defect on the tube, ν is a constant resembling the attempt frequency in a thermally activated process, and k_B the Boltzmann constant. In equilibrium, the defect density per site or per C-C bond only depends on the defect formation energy, E_d, given by $\rho(T)=(1+e^{E_d/k_B T})^{-1}$ after imposing a detailed balance of the creation and annihilation processes. There are different types of defects that could be thermally activated. From the literature,[22] we know that for planar graphene layers or CNTs with large cross sections, the two most common types of defects, vacancy and SW defects, have the formation energies of 7.8 and 10.4 eV, respectively.[23] These high formation energies suggest that the corresponding defect densities are entirely negligible even at the high temperature of $\approx$3000 K. Nevertheless, the formation energies can depend strongly on the curvature of the carbon nanomaterials, as already suggested for the case of conventional CNTs.[24] We have carried out systematic studies of such curvature dependences for both types of defects using LDA-DFT approaches. For the SW defects, the formation energy decreases exponentially as the curvature increases, and the dependence can be well fitted using the relation $E_d=E_0(e^{-K_l/c_1}+e^{-K_l/c_2})$, where $E_0=5.196$ eV, $c_1=0.029$, and $c_2=0.002$ (for the zigzag and armchair CNTs), giving a formation energy of less than 2 eV for $K_l>0.03$. In contrast, the formation energy of the vacancy defects has a weaker dependence on the curvature, and is still $\sim$5 eV even for a CNT with the smallest radius. Therefore, even at high temperatures and with large curvatures, only the SW defects can have a noticeable density.

Now we evaluate the contribution to the free energy due to the configuration entropy associated with the creation of the SW defects. When N_d defects are introduced to an N-atom system, there are Ω ways to distribute them, given by $\Omega=N!/[N_d!(N-N_d)!]$. For large N, the corresponding entropy increase is $S_d=-0.5k_B N[\rho \ln \rho+(1-\rho)\ln(1-\rho)]$, and the defect density is $\rho=N_d/(N/2)$ (the factor 1/2 reflects that only $N/2$ bonds are available for the creation of SW defects). For SWCNTs, the polygonal structures are energetically more costly because of the strain energy associated with the polygonization, but have higher entropies due to lower defect formation energy. Therefore, the competition between internal energetics and defect formation will determine the relative stability of the SWCNTs at a given temperature. Quantitatively, we have for the total free energy $F=\Delta E_{pol}+E_d N_d - TS_d$, where the internal energy ΔE_{pol} is different for different shapes of the CNTs [Eq. (2)], while the second term reflects the formation energy of the SW defects.

Figure 3(a) shows the total free energy of SWPNTs per unit length relative to that of the conventional (or circular) CNTs as a function of the local curvature at the tube circumference $W=2000$ nm. These plots define two critical temperatures, T^* and T_c. When $T\leqslant T^*=960$ K, the conventional

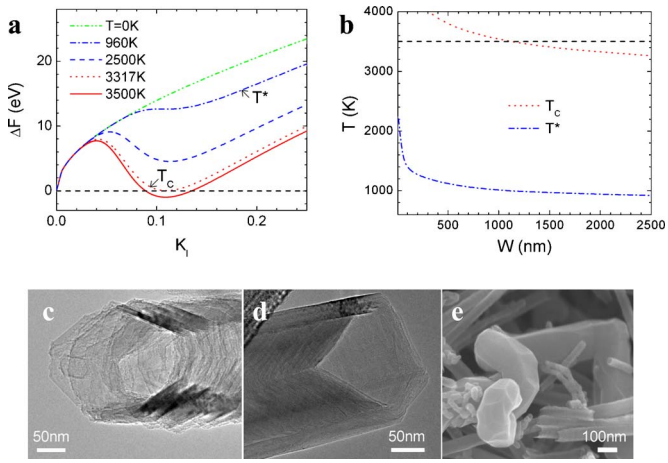

FIG. 3. (Color online) (a) Total free energy of single-wall polygonal nanotubes per unit length relative to that of the conventional (or circular) carbon nanotubes as a function of the local curvature at the tube circumference $W=2000$ nm. (b) Dependence of the two critical temperatures on W. TEM images [(c) and (d)] and SEM image (e) confirm the polygonization of the nanotubes upon high-temperature heat treatment ($T\geqslant 2800$ K).

nanotubes are globally stable, with no existence of other metastable structures. When $T^*<T<T_c$, the conventional nanotubes are still the stable structure, but the PNTs become metastable. Such metastable configurations can be reached kinetically at sufficiently high temperatures, but the polygonization process may take a very long time to reach because of the high activation barrier. When $T\geqslant T_c=3317$ K, the PNTs become stable globally, as indicated by the red solid curve in Fig. 3(a). In this regime, the heptagonal structure ($N_p=7$) is the most stable, while the hexagonal structure ($N_p=6$) is also more stable than conventional CNTs. Figure 3(b) illustrates the dependence of the two critical temperatures on the tube circumference. CNTs with large cross sections can be polygonized at sufficiently high temperatures, while those with small cross sections cannot, even at the high temperature of 3500 K, because of the existence of high (over 12 eV) kinetic barriers to reaching the metastable or stable polygonal states.

So far we have limited ourselves to the case of single-walled CNTs. When MWCNTs are considered, we expect that the stronger interlayer attractions among the layers [see Fig. 2(b)] will not only reduce the two critical temperatures for a given average W, but even more importantly, will also further stabilize the polygonal structures once they are achieved thermally. Qualitatively, this latter point suggests a hysteresis effect in the structural order versus temperature plot, but at this point a reliable quantitative description of this intriguing possibility is beyond the scope of the present work, as it would demand first-principles modelings of the MWCNTs and MWPNTs for large W. We further found that the existence of SW defects may also induce a slight reduction in the interlayer spacing, but for this effect to be comparable to the curvature-induced reduction, the defect density has to be unphysically high.

V. EXPERIMENTAL CONFIRMATION OF POLYGONIZATION

The predicted polygonal deformation of the MWCNTs with large circumferences upon high-temperature heat treatment has been confirmed by additional TEM and SEM studies of the heat-treated samples, particularly near the ends of the fibers. Here we compare the image of as-grown nanofibers and those heat treated to $T \approx 3250$ K. The SEM image of the as-grown samples displays circular structures [Fig. 1(a)]. In contrast, the cross section TEM [Figs. 3(c) and 3(d)] and SEM [Fig. 3(e)] images of the heat-treated nanofibers display distinct polygonal structures. These polygonally deformed samples are multilayered ($N_w > 20$) and have diameters in the range of 50–100 nm. On the other hand, samples with diameters less than 30 nm show d_{002} of 0.3427 (±0.0003 nm) and 0.3397 (±0.0002 nm) before and after heat treatment to 3100 K, respectively; the latter spacing is still greater than the graphite interlayer spacing of 0.3354 nm. Furthermore, no polygonization has been observed for such small-diameter samples.

Before closing, we note that observations of polygonization had been reported previously for bundles of SWCNTs under high hydrostatic pressure[25] and for large MWCNTs,[26] yet the physical origin(s) of the observed polygonization in these experiments was not fully explored.

VI. CONCLUSIONS

In conclusion, we have shown experimentally that polygonization of multi-walled carbon nanotubes or nanofibers can be induced at sufficiently high heat-treatment temperatures and with sufficiently large diameters. These trends are consistent with the predictions of a unified picture of carbon nanotubes and carbon polygons, developed through multiscale simulations rooted in extensive first-principles calculations. One central finding is the stabilization of polygonal shapes at high temperatures by the configuration entropy associated with the creation of the Stone-Wales defects. As a consequence of the polygonization, the interlayer spacing of the MWPNTs contracts to a value distinctly smaller than the established graphene interlayer spacing, as also confirmed theoretically. We expect that the phenomena of polygonization and potential interlayer spacing reduction established here for the MWCNTs will be applicable to other related tubular and/or fiber systems as well, such as BN nanotubes or nanofibers.[27]

ACKNOWLEDGMENTS

This work was supported by the U.S. Department of Energy (Grant No. DE-FG02-03ER46091 and the Division of Materials Sciences and Engineering, Office of Basic Energy Sciences, under Contract No. DE-AC05-00OR22725 with Oak Ridge National Laboratory, managed and operated by UT-Battelle, LLC), the HTML User Program, Assistant Secretary for Energy-Efficiency and Renewable Energy, Office of FreedomCAR and Vehicle Technologies, and the Laboratory Directed Research.

[1] H. W. Kroto, J. R. Heath, S. C. O'Brien, R. F. Curl, and R. E. Smalley, Nature (London) **318**, 162 (1985).
[2] S. Iijima, Nature (London) **354**, 56 (1991).
[3] R. E. Franklin, Acta Crystallogr. **4**, 253 (1951); G. E. Bacon, *ibid.* **4**, 558 (1951); W. Ruland, *ibid.* **18**, 992 (1965); P. L. Walker, *ibid.* **180**, 1184 (1957).
[4] B. T. Kelly, *Physics of Graphite* (Applied Science, London, 1981).
[5] J. Biscoe and B. E. Warren, J. Appl. Phys. **13**, 364 (1942); S. Iijima, Chem. Scr. **14**, 117 (1978).
[6] C. H. Kiang, M. Endo, P. M. Ajayan, G. Dresselhaus, and M. S. Dresselhaus, Phys. Rev. Lett. **81**, 1869 (1998).
[7] P. L. Walker and G. Imperial, Nature (London) **180**, 1185 (1957).
[8] P. J. Pappano, F. Rusinko, H. H. Schobert, and D. P. Struble, Carbon **42**, 3007 (2004).
[9] A. Nakayama, S. Iijima, Y. Koga, K. Shimizu, K. Hirahara, and F. Kokai, Appl. Phys. Lett. **84**, 5112 (2004); F. Banhart and P. M. Ajayan, Nature (London) **382**, 433 (1996); F. P. Bundy and J. S. Kasper, J. Chem. Phys. **46**, 3437 (1967); Y. X. Zhao and I. L. Spain, Phys. Rev. B **40**, 993 (1989); S. Scandolo, M. Bernasconi, G. L. Chiarotti, P. Focher, and E. Tosatti, Phys. Rev. Lett. **74**, 4015 (1995).
[10] The cooling rate is the natural cooling rate of a furnace; it takes 18–24 h to reduce the temperature from 3000 °C to room temperature, corresponding to 3 °C per 10 min.
[11] J. Peng, Q. Li, M. Zhou, and C.-C. J. Kuo, Proceedings of the Human Vision and Electronic Imaging VIII, IS&T/SPIE's 15th Annual Symposium for Electronic Imaging 2003: Science & Technology, Santa Clara, CA, 2003 (unpublished).
[12] J. M. Zuo, I. Vartanyants, M. Gao, R. Zhang, and L. A. Nagahara, Science **300**, 1419 (2003).
[13] G. Kresse and J. Furthmuller, Phys. Rev. B **54**, 11169 (1996).
[14] D. Vanderbilt, Phys. Rev. B **41**, R7892 (1990).
[15] D. M. Ceperley and B. J. Alder, Phys. Rev. Lett. **45**, 566 (1980).
[16] J. P. Perdew and A. Zunger, Phys. Rev. B **23**, 5048 (1981).
[17] H. J. Monkhorst and J. D. Pack, Phys. Rev. B **13**, 5188 (1976).
[18] H. Rydberg, M. Dion, N. Jacobson, E. Schröder, P. Hyldgaard, S. I. Simak, D. C. Langreth, and B. I. Lundqvist, Phys. Rev. Lett. **91**, 126402 (2003); H. Rydberg, N. Jacobson, P. Hyldgaard, S. I. Simak, B. I. Lundqvist, and D. C. Langreth, Surf. Sci. **532**, 606 (2003).
[19] M. Hasegawa and K. Nishidate, Phys. Rev. B **70**, 205431 (2004), and references therein.
[20] F. D. Murnaghan, Proc. Natl. Acad. Sci. U.S.A. **30**, 244 (1944).
[21] O. Zhou, R. M. Fleming, D. W. Murphy, C. H. Chen, R. C. Haddon, A. P. Ramirez, and S. H. Glarum, Science **263**, 1744 (1994); Y. Maniwa, R. Fujiwara, H. Kira, H. Tou, E. Nishibori, M. Takata, M. Sakata, A. Fujiwara, X. Zhao, S. Iijima, and Y. Ando, Phys. Rev. B **64**, 073105 (2001); Y. W. Fan, B. R. Goldsmith, and P. G. Collins, Nat. Mater. **4**, 906 (2005).
[22] E. Kaxiras and K. C. Pandey, Phys. Rev. Lett. **61**, 2693 (1988).

[23] Here the vacancy formation energy is obtained by removing a carbon atom from an ideal carbon nanostructure and adding it to the inner region of a structure of the same kind, while the SW defect formation energy is obtained by rotating a C-C bond by 90°; see M. Yoon *et al.*, Phys. Rev. Lett. **92**, 075504 (2004).
[24] T. Dumitrica and B. I. Yakobson, Appl. Phys. Lett. **84**, 2775 (2004).
[25] J. Tang, L.-C. Qin, T. Sasaki, M. Yudasaka, A. Matsushita, and S. Iijima, Phys. Rev. Lett. **85**, 1887 (2000).
[26] M. Q. Liu and J. M. Cowley, Ultramicroscopy **53**, 333 (1994).
[27] N. G. Chopra, R. J. Luyken, K. Cherrey, Vincent H. Crespi, Marvin L. Cohen, Steven G. Louie, and A. Zettl, Science **269**, 966 (1995).
[28] J. Y. Howe, G. G. Tibbetts, C. Kwag, and M. L. Lake, J. Mater. Res. **21**, 2646 (2006).